

## Deep spontaneous penetration of a water droplet into hot granular materials

Fangye Lin

*Ningbo Research Institute, Zhejiang University, Ningbo 315048, China  
and State Key Laboratory of Fluid Power and Mechatronic Systems, Zhejiang University,  
Hangzhou 310027, China*

Stéphane Dorbolo <sup>\*</sup>

*FNRS-CESAM-GRASP, Département de Physique, Université de Liège, B-4000, Belgique*

Wei Wang and Jun Zou <sup>†</sup>

*State Key Laboratory of Fluid Power and Mechatronic Systems, Zhejiang University,  
Hangzhou 310027, China*



(Received 17 August 2021; accepted 22 February 2022; published 21 March 2022)

The Levitation of a droplet on a hot surface due to the rapid vaporization of the liquid at the proximity of the heat source is known as the Leidenfrost effect. This effect has been demonstrated when the surface is a solid or a liquid. Here, we explore the interaction between a liquid droplet and a hot granular material. The granular material is, by essence, a solid but adopts some behaviors similar to fluids. Surprisingly, we found that the droplet deeply penetrated the hot granular material. During the penetration process, the vapor production is so intense that the grains underneath the droplet are ejected. Consequently, the droplet moved downward under the action of gravity. A mechanism based on the Leidenfrost effect is proposed considering that the granular material can be modeled as a rough surface that can be eroded when the vapor speed is sufficient.

DOI: [10.1103/PhysRevFluids.7.034301](https://doi.org/10.1103/PhysRevFluids.7.034301)

### I. INTRODUCTION

When a liquid droplet meets a hot solid, the resulting heat transfer can be high enough to provoke the continuous vaporization of the droplet. Under these conditions, a vapor film separates the liquid and the solid, which is referred to as the Leidenfrost effect [1–4]. The conditions that affect the boiling temperature toward the Leidenfrost state depend on the nature of the liquid (mostly the transition temperature and latent heat), the nature of the solid (the thermal conductivity must be high enough to allow the rapid heat transfer to the droplet), and the geometrical configuration (the shape and surface roughness of the solid). The Leidenfrost effect is an important issue regarding cooling processes. When a surface is heated to an extreme temperature, the cooling efficiency of water is drastically reduced by the formation of a vapor layer between the droplet and solid, thereby inhibiting cooling. This effect was critical during the Fukushima nuclear accident [5]. Increasing the roughness of the surface is one way to increase the Leidenfrost transition temperature [6].

The Leidenfrost transition temperature corresponds to the liquid-vapor transition temperature of the droplet when the solid is substituted by a hot liquid, for example, in a bath of hot oil [7]. The

---

\*s.dorbolo@uliege.be

†junzou@zju.edu.cn

bath surface remains smooth up to the molecular scale. Nevertheless, the thermal conductivity of liquids is lower than that of metals. This low conductivity is compensated by the convective flows inside the liquid triggered by surface cooling and the bulk flows induced by the droplet and vapor entrainment [8].

Granular materials are known to share some properties with solid, liquid and gas [9], consequently the Leidenfrost effect on a granular bed is questioned. Along the same line, one may question the ability of droplets to cool granular soils [10]. First, it is acknowledged that after the passage of wildfires, affected soils are hydrophobic, and any droplets impacting these soils are covered by a thin layer of dust particles [11]. As a consequence, water does not penetrate these soils. It is expected that this behavior may occur during fire extinction. In addition, granular materials are poor thermal conductors because the contact between grains is characterized by a high thermal resistance. In a recent report, the thermal conductivity of an assembly of steel beads was found to be 100 times lower than this of the bulk steel [12]. The same was reported in thermal conductivity measurements of glass beads which size was between 100 and 200  $\mu\text{m}$  (with a certain dependence on the size) [13].

Regarding the Leidenfrost effect, granular materials are considered unsuitable candidates to trigger Leidenfrost transition. The following three reasons have been identified: (i) the surface of a granular material is very rough, (ii) the poor thermal conductivity of the granular assembly does not guarantee that heat is transferred fast enough to sustain the intervening vapor film, and (iii) grains may move under the action of the droplet and may even become trapped by the droplet as observed at room temperature [14–16] and high temperatures [10,17]. In contrast, direct contact (trapping) with grains facilitates rapid heat transfer to the droplet, which could yield a high rate of vapor production.

In this work, we present original experiments, in which a droplet is gently dropped on a heated granular material. Within a given temperature range, we find that the droplet penetrated into the granular material. The droplets are then able to reach depths up to 15 times their diameter. This surprising phenomenon is described and explained.

Two experimental setups were designed for examining the impact of a room temperature water droplet on a heated granular bed. The first 3D, cylindrical setup consisted of a thick cylinder filled with grains. Actually, we will observe that the droplet disappears for a given range of temperature. That is the reason why a second setup, which is quasi-2D, was designed. This setup consisted of a Hele-Shaw cell, in which one wall was composed of sapphire to directly observe the droplet motion inside the granular material. This system allowed us to observe the motion of the droplet and grains thanks to a transparent window of sapphire. The bed temperature  $T_b$  varied between 100°C and 450°C.

## II. EXPERIMENTAL DETAILS

### A. Grains

The used silicon carbide (which density  $\rho_g = 3.2 \text{ g/cm}^3$ ) grains are produced by Mingzhi Abrasive (China). Three kinds of grains were used and named SiC-I, SiC-II, and SiC-III (see Table I). The grains were characterized using a laser particle size analyser (Mastersizer 2000, Malvern Instruments). The particles have irregular shapes as shown in Fig. S1 [18]. The distribution of the size is monomodal (see Table S1 [18]). Since these grains are mostly nonspherical, we used surface-area based mean diameters as the characteristic diameter, i.e.,  $d_g = d_{3,2} = 28, 40, \text{ and } 55 \mu\text{m}$  for three types of SiC powder, respectively (see the definition of  $d_{3,2}$  in the caption of Table SI [18]).

The thermal conductivity of the granular material was measured by a thermal conductivity measurement device (TPS 3500, Sweden). At room temperature, the thermal conductivity  $\kappa_g$  for SiC-I, SiC-II, and SiC-III was found to be 0.204, 0.203, and 0.208 W/(m K), respectively, which seems independent of the grain size. As the temperature increase,  $\kappa_g$  increases slightly:  $\kappa_g$  is

TABLE I. Properties of grains.

Sample	Diameter		Thermal conductivity (T=20°C)		Packing fraction		Density
	$d_g$ ( $\mu\text{m}$ )		$\kappa_g$ (W/(m K))		2D	3D	$\rho_g$ (kg/m <sup>3</sup> )
					$\phi$		
SiC-I	28		0.204				
SiC-II	40		0.203		0.39±0.01	0.42±0.02	3200
SiC-III	55		0.208				

0.230 and 0.245 W/(m K) for SiC-I at 100 and 200°C (the highest temperature that the thermal conductivity can reach), respectively. In the 2D/3D experiments, the bed temperature ranges from 200 to 450°C. The thermal conductivity  $\kappa_g$  in this work is estimated to  $\kappa_g = 0.25$  W/(m K). As expected, this value is several order of magnitude lower than the bulk SiC material ( $\kappa_b = 234$  W/(m K) [19]) since the obtained grain contact does not facilitate thermal conduction and since air is present in the packed granular bed.

The estimated contact angle with water of the solid particles ranges from 70–90°. Superhydrophobic SiC particles are prepared by coating normal particles with silica nanoparticles. A commercial agent (Glaco Mirror Coat Zero, Soft 99 Co.) is applied for particle coating purposes. The estimated contact angle with water of the superhydrophobic particles ranges from 110–120°.

## B. Experimental setups

The 3D experiments were based on a cylindrical granular packed bed placed on a thermostatic heater Fig. 1(a). To obtain this granular packed bed, particles were poured into a hopper and freely filled a cylindrical aluminium container (depth = 10 mm, inner diameter = 31 mm, and wall thickness = 2 mm). The granular packed bed in the container was leveled with a microscope slide. The packing fraction was  $\phi = 0.42 \pm 0.02$ .

The granular beds were then heated to the target temperature with a thermostatic heater for more than 30 min. Various surface temperatures ( $T_s = 25$ –300°C) were achieved by controlling the thermostatic heater from 25–450°C. The temperature stabilization was verified with a thermocouple. Note that a temperature gradient still existed and was measured between the surface of the granular bed and the interior (see Supplemental Material Sec. S2 [18]). The average temperature of the top of the granular bed  $T_s$  was chosen as the characteristic temperature. The superheat  $\Delta T$  was defined as the difference between the actual temperature  $T_s$  and the boiling point of water  $T^* = 100^\circ\text{C}$ . After the thermal stabilization, a droplet was released 10 mm above the surface of the granular material and filmed at an angle of approximately 45°. The droplet radius  $R$  was 1.4 mm. Eventually, the droplet behavior was recorded with a high-speed camera (Phantom V2512) at 50–2000 frames per second (fps).

The quasi-2D granular beds were based on a Hele-Shaw cell with a dimension of  $42 \times 45 \times 3$  mm [shown in Figs. 2(a) and 2(b)]. The cell was backed onto an aluminium block which had four heating tubes, i.e., the aluminium block functioned as a thermostatic heater, which regulated the bed temperature  $T_b$  from 100 to 450°C. The front side of the cell was made of a sapphire window, allowing a side view of the digging process. The cell was first filled by particles, and an electromagnet shaker was used to vibrate the aluminium container, which consequently adjusted the packing fraction of the granular bed. The packing fraction was  $\phi = 0.39 \pm 0.01$  in the present work.

This system allowed us to observe the motion of the droplet and grains due to a transparent window consisting of sapphire. The bed temperature  $T_b$  varied between 100°C and 450°C. The temperature distribution in the granular packing was homogeneous, as shown in the Supplemental Material (Sec. S2) [18].

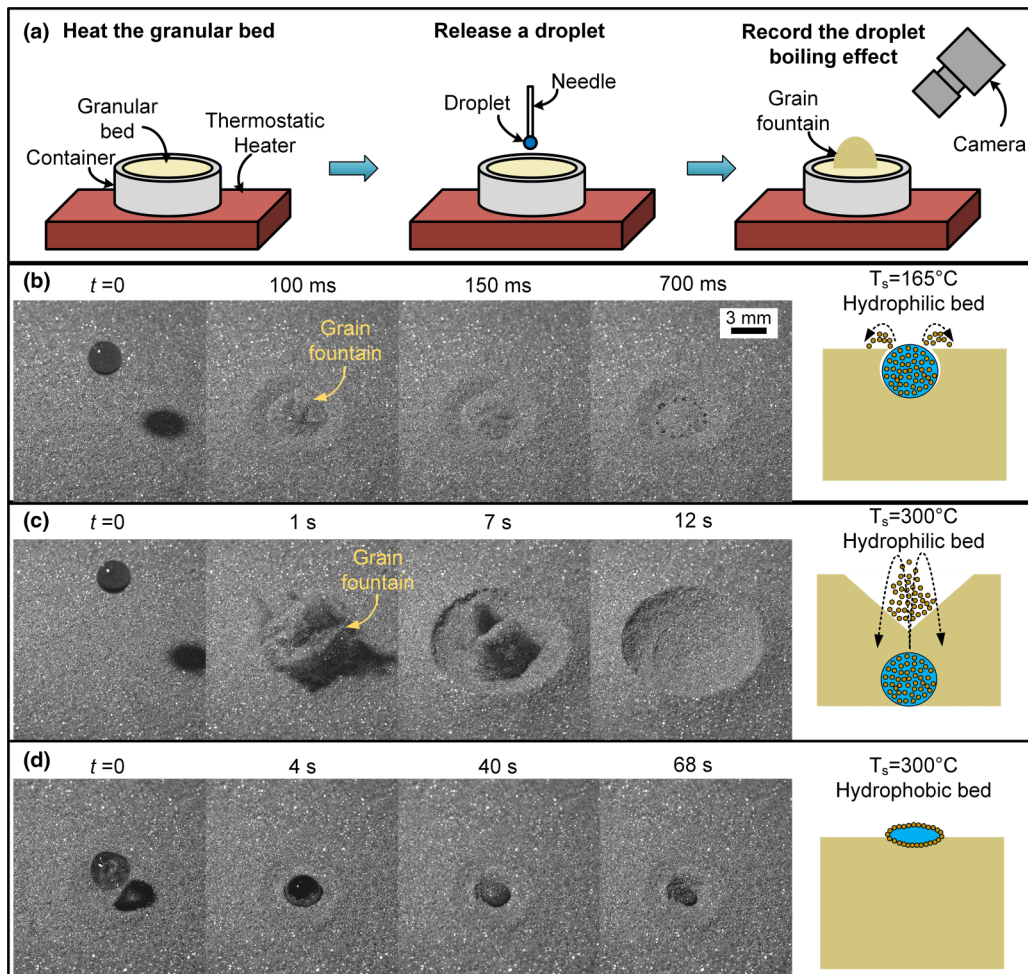


FIG. 1. (a) 3D setup: A cylindrical container was filled with SiC grains (SiC-III). The temperature was controlled with a thermostatic plate. The penetration of the water droplet was recorded with a high speed camera under an angle of  $45^\circ$ . (b) A drop released onto a hydrophilic granular bed at  $T_s = 165^\circ\text{C}$  (regime I). The sand boiling effect was observed as a grain fountain nearly instantaneously occurred after contact between the droplet and grains. The droplet boiled near the interface of the bed. When the grain fountain settled (nearly 700 ms), small holes remained at the surface. They were found along the initial perimeter of the droplet and were regularly spaced. (as shown in the fourth image in panel (b) and Movie S2 [18]). (c) The grain bed ( $d_g = 55 \mu\text{m}$ ) was heated up to a temperature of  $T_s = 300^\circ\text{C}$ . Water was completely vaporized after 12 s. After the complete vaporization of the droplet, a large amount of grains was expelled across a long distance from the impact. A crater was then obtained after the full vaporization of the droplet (please refer to Movie S3 [18]). In both cases, panels (b) and (c), a spherical assembly of grains was found below the surface (see Fig. S5). (d) As a comparison, the same grains were coated with hydrophobic molecules ( $T_s = 300^\circ\text{C}$ ). Because of this treatment, the water droplet no longer penetrated the surface of the granular material (as shown in Movie S5 [18]).

### III. DROPLET ON THE HOT GRANULAR PACKED BED

The nature, size, and shape of the grains are important parameters. We chose silicon carbide grains because of the high thermal conductivity of SiC bulk ( $\kappa_b = 234 \text{ W}/(\text{m K})$  [19]) compared

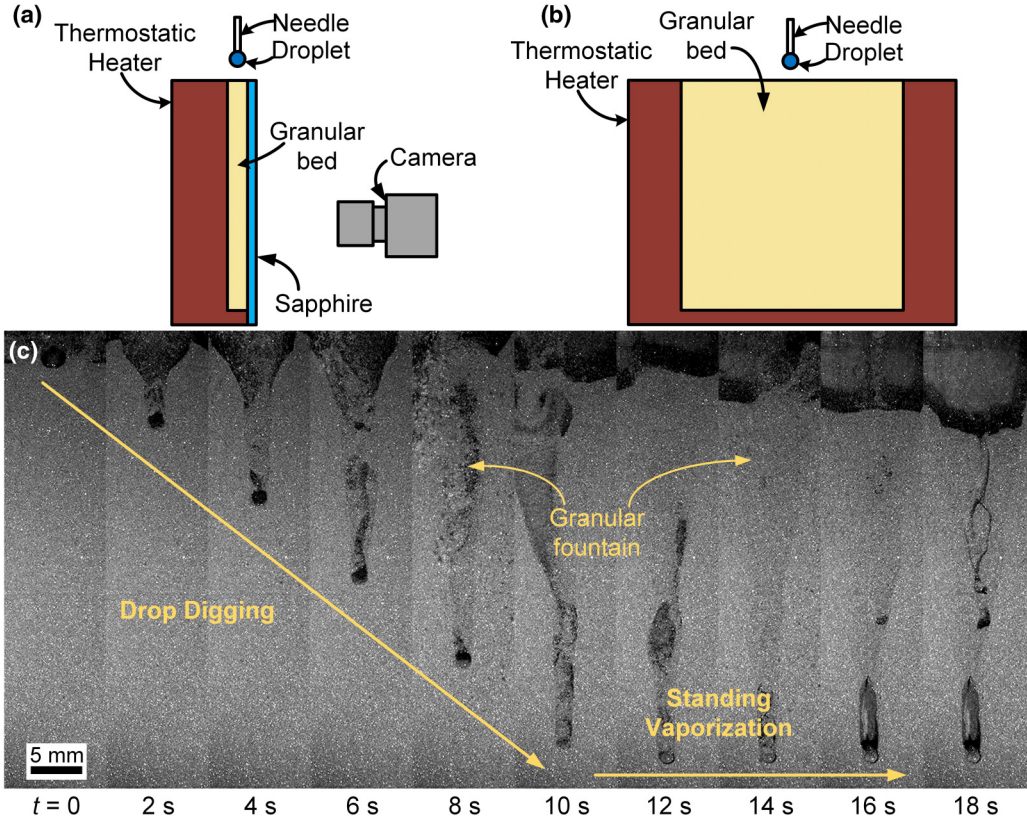


FIG. 2. (a) Side view of the 2D setup: A Hele-shaw cell was constructed and filled with SiC grains. One of the vertical walls was heated and maintained at a constant temperature, while the opposite wall consisting of sapphire enabled us to record the motion of the droplet below the surface with a high speed camera. (b) Front view of the 2D setup. (c) Time lapse of a typical penetration process (also shown in Movie S6 [18]). The temperature of the granular bed was  $T_b = 300^\circ\text{C}$ . The pictures are separated by 2 s. The maximum digging depth was  $H_{\text{max}} = 39.0$  mm. The droplet moved at a constant speed until  $t = 10$  s. Above the droplet, the granular bed was fluidized along a vertical cylinder whose diameter corresponded to the diameter of the droplet until 10 mm below the surface. Then the fluidized granular part formed a funnel at the surface, i.e., the crater. The crater diameter increased over time. At  $t > 10$  s, the droplet no longer moved downward. The grains remained fluidized until the complete vaporization of water.

to sand [ $\text{SiO}_2$  thermal conductivity is about  $2 \text{ W}/(\text{m K})$ ] and even iron [about  $80 \text{ W}/(\text{m K})$ ]. However, the thermal conductivity of an assembly of SiC grains was measured to be  $\kappa_g = 0.25 \text{ W}/(\text{m K})$  which sharply contrasts with the bulk as already observed in Refs. [12,13]. Three sizes of grains were considered named SiC-I, SiC-II, and SiC-III which differ by their diameter  $d_g = 28, 40,$  and  $55 \mu\text{m}$ .

#### A. What can be observed from the top

Let us first consider the 3D case. The 3D experiments were based on a cylindrical granular packed bed placed on a thermostatic heater Fig. 1(a). The granular beds were then heated to the target temperature. A droplet ( $R = 1.4$  mm) was gently released onto a granular bed. Comparing to room temperature interaction (please refer to Movie S1 [18]), the drop-grain interaction on the heated granular bed was highly violent. The liquid was heated upon direct contact with the hot

particles, and a strong vapor flow was generated, which expelled particles into the air, thus forming a grain fountain (as shown in Figs. 1(b) and 1(c) (second image); please also refer to the Movies S2 and S3 [18]). Particle ejection occurred when the average temperature of the bed surface  $T_s$  was higher than the boiling temperature of water.

According to the temperature, two regimes were characterized based on the final pattern observed at the surface of the granular bed. The patterns are shown in the fourth panel of Figs. 1(b) and 1(c).

Regime I [Fig. 1(b)]: For  $100^\circ\text{C} \leq T_s \leq 165^\circ\text{C}$ , the droplet penetrates into the granular material and disappears under a fountain of grains. In this regime, the grain fountain is mainly located along the edge of the droplet (please also refer to Movie S2 [18]). This behavior is similar to what has been observed for a thin layer of grains (of the order of the droplet diameter) in Ref. [10]: the generated vapor expels any surrounding grains. Moreover, in the present case, the droplet may disappear under the surface of the granular material. When the droplet is completely evaporated, a chain of holes is formed at the surface of the granular material. The chain size corresponds the drop diameter, as shown in Fig. 1(b) [the grain (SiC-III) size is  $d_g = 55 \mu\text{m}$  and the bed temperature is  $T_s = 165^\circ\text{C}$ ]. The chain of holes results from the upward motion of the vapor and the downward motion of the grains. A wavelength is selected that corresponds to the size of the vapor bubbles.

The grains surrounding the fountain were gently removed to uncover the remaining of the droplet. Actually, after the complete evaporation, we could extract an assembly made of the grains gathered by the droplet. This assembly was partly exposed to air or was covered by a few layers of particles. The fragile but coherent assembly of grains can be observed (please refer to Supplemental Material Sec. S3 [18]).

Regime II [Fig. 1(c)]: At  $T_s > 165^\circ\text{C}$ , upon contact of the droplet with the grains, a very large fountain of grains is generated. Particle ejection leads to a crater whose size increases because of the continued collapse of the crater edge. The droplet penetrates the granular material and then disappears below the surface. Figure 1(c) shows the formation of a large crater at  $T_s = 300^\circ\text{C}$  considering the same grains as in Fig. 1(b). In contrast to regime I, a cohesive assembly of grains resulting from droplet evaporation is encountered deep inside the granular bed (in the example, particle collection occurs at the bottom of the container at  $T_s = 300^\circ\text{C}$  and  $d_g = 55 \mu\text{m}$ ). However, the shape of the assembly remains spherical (please refer to Movie S4 [18]). In both regimes, the obtained assembly is a sphere with a diameter very close to the diameter of the initial droplet.

Grains were also coated to make their surface superhydrophobic. The interaction of the droplet with superhydrophobic grains at fixed temperature of  $300^\circ\text{C}$  is shown in Fig. 1(c). In this case, no boiling is observed. A monolayer of grains covers the droplet until it is fully covered ( $t = 40$  s). The granular shell collapses. The absence of fountain clearly demonstrates that the contact with the grains is a primordial to observe a fountain and the fast production of vapor.

## B. What can be observed below the granular surface

The 3D granular bed experiments provide a global view of the interaction between the droplets and a high-temperature granular bed. However, the experimental setup does not reveal what occurs inside the granular bed. To better understand the interaction between the droplet and the heated granular bed, quasi-2D experiments are necessary. The 2D setup was limited due to the occurrence of the sapphire window. Indeed, the bed temperature  $T_b$  must be set to a value higher than the Leidenfrost point relative to the sapphire window (nearly  $200^\circ\text{C}$ ). Otherwise, the droplet contacts the sapphire wall. As a consequence, only the regime II can be examined with this device.

A droplet penetrating the granular material is shown in Fig. 2(c) (please also refer to Movie S6 [18]). The bed temperature is set to  $T_b = 300^\circ\text{C}$  and the grain size is  $d_g = 28 \mu\text{m}$  (SiC-I). As the droplet contacts the granular bed ( $t = 0$ ), some particles were absorbed by the drop. Moreover, vaporization of the liquid generated a strong vapor flow that expels particles upward initially located underneath the droplet. The ability to remove underlying particles implies that the droplet moves downward: the droplet penetrates the granular bed. The resultant vapor flow entrains bed particles, which feeds the grain fountain. Actually, we observe that the granular material was fluidized from

the top of the droplet to the surface. The fluidized region exhibits a cylindrical shape from the top of the droplet to approximately 10 mm below the initial surface of the granular bed. Above this limit, a granular crater developed.

The droplet progresses at an approximately constant speed of  $v_0 \approx 4$  mm/s between  $t = 0$  to  $t = 10.4$  s and then suddenly stops at a depth that was approximately 14 times the droplet diameter [Fig. 3(a)]. However, the grain fountain continues expelling grains for another 7 s after droplet stops progression. It should be noted that during the penetration process, an increasing number of particles is absorbed by the droplet. This leads to the formation of a particle agglomeration, which was also found in the 3D granular bed experiments. The liquid drop is saturated with particles; at that moment, the penetration stops.

The position  $H$  ( $H = 0$  corresponds to the surface) of the droplet is plotted as a function of time at different temperatures in Fig. 3(a). The last point of each curve corresponds to the end of droplet vaporization, i.e., when the fountain stops (please refer to Movie S7 [18]). The dynamics are decomposed into three steps: air-grains interface crossing, digging, and standing vaporization. First, the droplet slowly crosses the air-granular material interface. Indeed, the interface is the coldest part of the granular bed (please refer to Supplemental Material Sec. S2 [18]). As soon as the droplet is below the surface, namely,  $H$  is on the order of the droplet diameter  $D$ , the penetration speed increases and remains constant until the final depth is reached [ $H$  is a linear function over time, as shown in Figs. 2(c) and 3(a)]. Additional curves for the particles SiC-II and SiC-III are shown in the Supplemental Material Sec. S4 [18]. During motion, particles are absorbed by the droplet. Finally, the droplet stops at a depth of  $H_{\max}$ , until the water is completely evaporated (standing vaporization regime).

Related to these three steps, three periods can be defined, namely,  $\tau_i$ , the time to cross the interface,  $\tau_d$ , the duration of the digging process at a constant speed  $v_d$  and,  $\tau_s$  the duration of the static regime. The sum of these three durations is equal to the lifetime of the droplet  $\tau = \tau_i + \tau_d + \tau_s$ . Note that vaporization may not necessarily cease after time  $\tau$  because there are no visible effects of evaporation. In other words, we determine  $\tau_s$  when motion around the “droplet is no longer observed.” These times are reported as a function of the superheat  $\Delta T$  (The superheat  $\Delta T$  was defined as the difference between the actual temperature  $T_b$  and the boiling point of water  $T^* = 100^\circ\text{C}$ ), as shown in Fig. 3(b). We observe that the total lifetime  $\tau$  remains roughly constant approximately 19 s. Interface crossing requires increasingly more time with increasing temperature. The penetration time ( $\tau_i + \tau_d$ ) linearly increases with  $\Delta T$ , and consequently,  $\tau_s$  decreases with increasing  $\Delta T$ . The increase in penetration time ( $\tau_i + \tau_d$ ) is, according to the observations, related to the decrease in the particle trapping rate with increasing the temperature (see Supplemental Material S5 for more details [18]).

The final depth  $H_{\max}$  reached by the droplet is governed by the average digging speed  $v_d$  and the duration ( $\tau_i + \tau_d$ ). The final depth and the digging speed are shown as a function of the superheat  $\Delta T$  in Fig. 3(c) for the three types of considered grains SiC-I, -II, and III. A maximum is observed for the SiC-I and SiC-II at  $\Delta T = 200^\circ\text{C}$ . The digging speed  $v_d(\Delta T)$  is estimated via a linear fit [dashed lines in Fig. 3(a)] on the  $H(t)$  between  $H = 2D$  and  $H = H_{\max}$  (Supplemental Material Sec. S4 [18]). The digging speeds are shown in Fig. 3(d) for the three kinds of grains (see the legend). We observe that (i) at high temperatures, the digging speed decreases approaching zero, and (ii) the digging speed increases with the grain size. In the following, we focus on the digging speed and how to explain the dependence on the temperature and the grain size. The final depth  $H_{\max}$  depends on the crossing time since we observe that the total lifetime does not depend too much on the temperature. The crossing time is a delicate problem because of the presence of a temperature gradient close to the surface.

#### IV. MODEL

Considering the empirical average vapor production  $Q_{\text{exp}}$  (based on the initial volume and on the penetration time, we can estimate the average speed of the vapor. If we assume that the digging

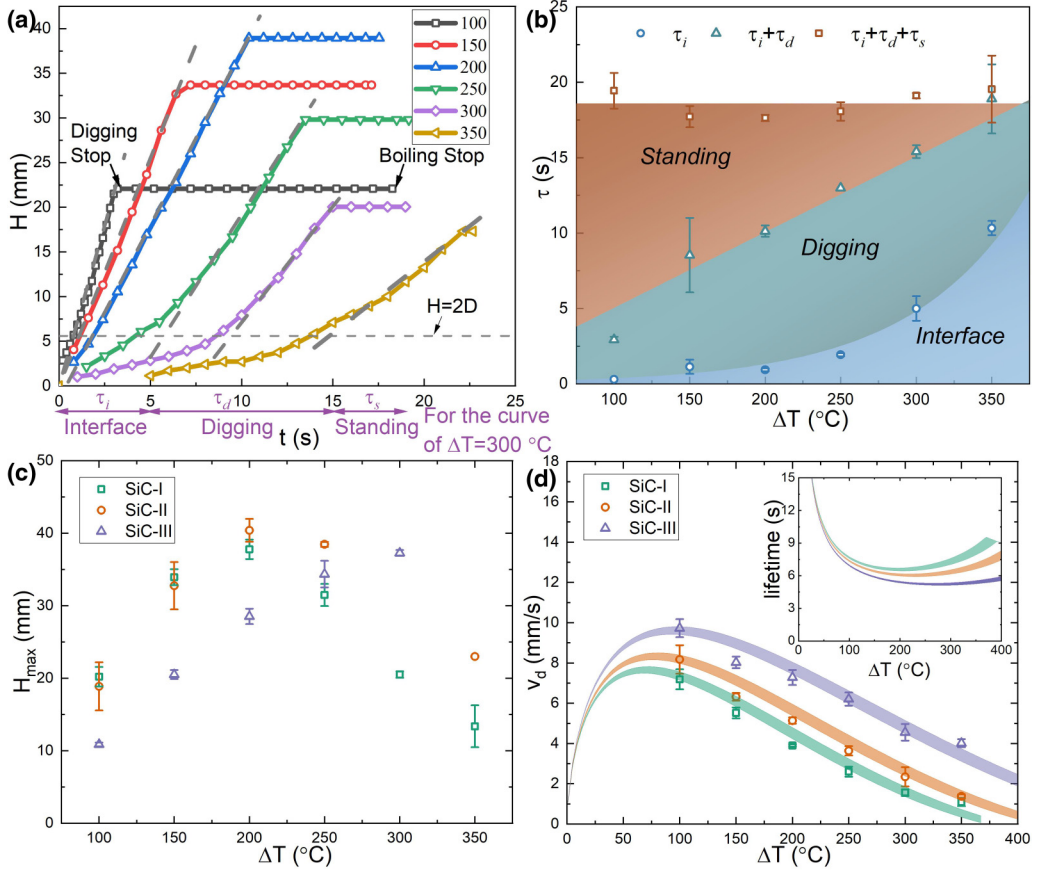


FIG. 3. (a) Depth reached by the droplet as a function of time at the different temperatures between 200 and 450 °C. The legend is corresponding to the superheat  $\Delta T = (T_b - T^*)$ , where  $T^* = 100$  °C is the boiling point of water. The grains are SiC-I grains (please refer to Supplemental Material Sec. S4 for information on the other types of grains [18]). Three steps are identified: the time to cross the interface  $\tau_i$ , the deep digging process during the time  $\tau_d$  and the standing state during  $\tau_s$ . As shown in purple in panel (a), the different step durations are indicated in the case of  $T_b = 400$  °C. (b) Distribution of the duration of the different steps ( $\tau_i$ ,  $\tau_d$ , and  $\tau_s$  are marked with the blue circles, blue triangles, and brown squares, respectively) during the digging process as a function of the superheat  $\Delta T$ . The total duration of the process remains constant. The time to cross the interface linearly decreases with the superheat. In contrast, since the standing time (or equivalently  $\tau_i + \tau_d$  linearly increases) reaches its maximum value at  $\Delta T = 250$  °C. (c) Based on the  $H(t)$ , the maximum depth reached by the droplet is determined. The blue squares, orange triangles and purple triangles indicate  $H_{\max}$  for the SiC-I, SiC-II, and SiC-III grains, respectively as a function of the temperature. (d) The speed  $v_d$  during the digging process is shown as a function the granular bed superheat. The symbols are the same as those in panel (c). The speed continuously decreases with the temperature. The curves correspond to the model described in Sec. IV considering  $r_{\text{rug}} = 69.5 \pm 0.5$ ,  $71.5 \pm 0.5$ , and  $75 \pm 0.5$   $\mu\text{m}$  for the SiC-I, SiC-II, and SiC-III, respectively. The predicted lifetime of the droplet is presented in the inset as a function of the superheat.

speed is proportional to the grains speed and that the average grains speed linearly depends on the vapor speed, then we found that the digging speed  $v_d \propto Q_{\text{exp}}^{2/3}$  (see Supplemental Material S6 [18]). The key now is to understand how the vapor production changes with the temperature.

Since no bubble is observed and since the droplet slowly evaporates regarding the temperature of the bath, we assume that the droplet does not boil during the digging process, but heat is transferred toward the droplet continuously. This situation is very similar to Leidenfrost state. We propose a mechanism for the digging process that is related to the Leidenfrost scheme. Due to the proximity of the droplet to the hot granular bed, under the action of the weight of the droplet  $F_w$ , water vapor is generated between the droplet and hot surface. If the substrate were a solid, then the created vapor would generate a thin vapor film. The thickness  $h$  of the film depends on the heat transfer occurring from the substrate to the droplet and on the size of the droplet. When the resulting heat transfer is sufficient, the compression attributed the vapor generates a sufficient vertical force via lubrication to balance the droplet weight [3,4]. In a granular bed, the speed  $v_v$  of the vapor generated by water vaporization may be also sufficient to eject the grains just underneath the droplet especially when the vapor is generated directly inside the granular material. The granular bed is thus locally fluidized, encouraging the droplet to move downward in the bed: The droplet digs. As we observed that the digging speed remains constant, the droplet reaches a steady state: Instead of producing a thin vapor film, the droplet sits on a layer of fluidized granular bed material and moves downward. The thickness of the fluidized bed depends on the heat transfer and on the geometry of the droplet.

A notable and empirical analogy can be drawn regarding the behavior of a droplet released on a very rough and hot surface. This study was performed by Kim [6]. To detect the temperature  $T_L$  above which a given droplet levitates on its own vapor, the lifetime of a droplet of a given volume was measured at different temperatures. On a smooth and high-thermal conductivity substrate such as copper, the lifetime first decreases until  $T_L$  is reached. Then, the lifetime steeply increased depending on the substrate properties. This steep increase corresponds to the sudden decrease in the heat transfer from the substrate to the droplet attributed to the presence of a vapor film. Kim observed the evolution of the droplet lifetime as a function of the temperature considering a rough substrate. In this case, the transition to the Leidenfrost state is no longer sharp, but the lifetime continuously increases between the water boiling temperature and the Leidenfrost temperature. The lifetime increase with the temperature means that the heat transfer from the substrate to the droplet keeps on decreasing when the temperature increases. This is due to the decrease of the contact area between the droplet and the substrate when the temperature of the substrate increases. Eventually, the Leidenfrost temperature is reached, and the vapor film thickness exceeds the roughness size of the substrate.

We propose to model the granular material by two phases: (i) the bulk which is topped by (ii) the surface layer. The phases are separated by a horizontal plane  $\Sigma_i$ . In the bulk phase, the thermal conductivity is a constant, namely, the thermal conductivity of the granular material  $\kappa_g$  (here, 0.25 W/K/m; see Sec. II). The bulk phase is topped by the surface layer which has a thickness  $r_{\text{rug}}$ . We model the surface layer by a 2D hexagonal compact assembly of so called “roughness” spheres with a radius  $r_{\text{rug}}$  larger than the grain size [the green sphere in Fig. 4(c)]. This surface layer accounts for the roughness of the granular material. Moreover, within this surface layer, the grains are allowed to move.

The thermal conductivity in the surface layer  $\kappa_{\text{eff}}$  is not constant but varies with the distance  $y$  to  $\Sigma_i$ . More precisely,  $\kappa_{\text{eff}}(y = 0) = \kappa_g$  [0.25 W/(m K)] at the interface  $\Sigma_i$  to the thermal conductivity of the water vapor  $\kappa_{\text{eff}}(y = r_{\text{rug}}) = \kappa_v$  [0.04 W/(m K)] at the top of the surface layer since the droplet is evaporating along this upper interface (grains-vapor interface). To determine the dependence of the effective thermal conductivity  $\kappa_{\text{eff}}$  on the distance  $y$  above the plane  $\Sigma_i$ , let us consider a plane  $\Sigma$  parallel to  $\Sigma_i$  and located at a distance  $y$  above  $\Sigma_i$ . Between the plane  $\Sigma_i$  and  $\Sigma$ , the heat is conducted through the grains and through the air located between the grains. To account for both heat conducting channels, the effective thermal conductivity of the material located between  $\Sigma_i$  and  $\Sigma$  is determined by considering the area of the spheres of radius  $r_{\text{rug}}$  intersected by the plane  $\Sigma$ . The intersection is made of discs with the same geometrical arrangement as that of the “roughness” spheres [the pink zones in Fig. 4(c)]. The intersection discs radius  $r^*$  is given by  $r^* = \sqrt{r_{\text{rug}}^2 - y^2}$ . The surface fraction  $x$  covered by the discs is obtained by dividing the half of the area of an

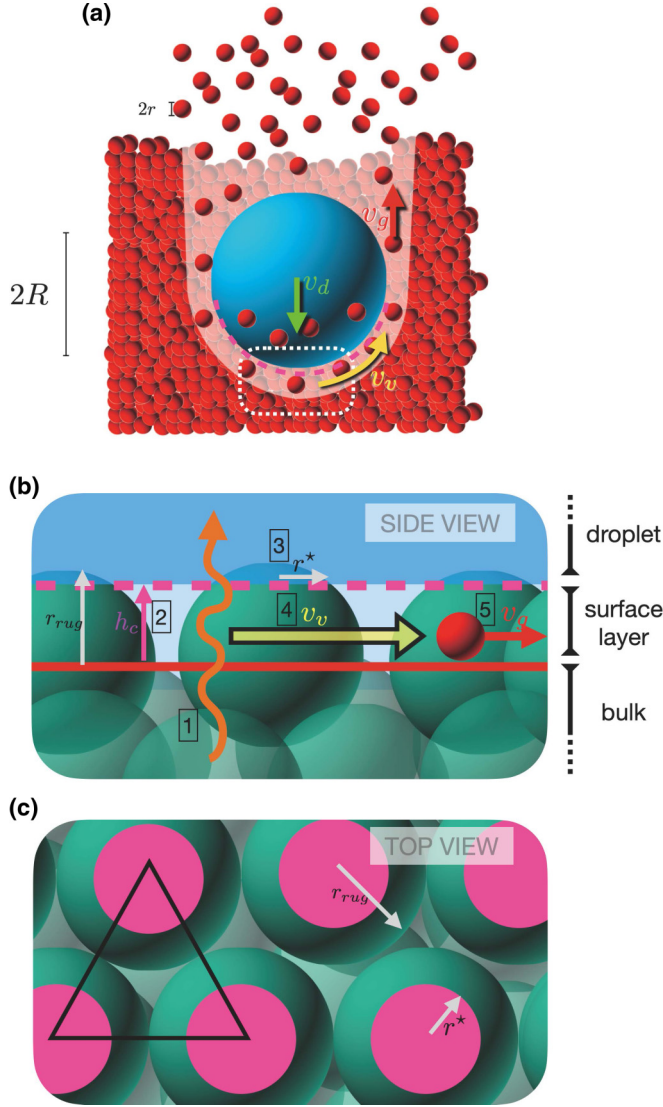


FIG. 4. (a) The digging droplet is modeled as a droplet surrounded by an air-grain mixed layer ejected under the action of the produced vapor. (b) Zoom of the side view of the film. The cyan spheres indicate the spheres (radius  $r_{\text{rug}}$ ) adopted to represent the roughness. Heat is transferred via conduction [1]. The purple dashed line indicates the height of the vapor film calculated on an idealistic smooth surface [2]. This line intersects the rough spheres [3]. The intersection with the spheres induces a supplemental amount of vapor that allows us to calculate the speed of the vapor  $v_v$  [4]. The vapor then entrains grains [5]. (c) Top view of intersection between the liquid and rough spheres. The contact is indicated as purple discs.

intersection disk by the surface of an equilateral triangle of base  $2r_{\text{rug}}$  [as shown in Fig. 4(c)], namely,  $x = \frac{\pi r^{*2}}{\sqrt{3}r_{\text{rug}}^2}$ . Since the heat is transferred by two parallel channels: through the vapor located between the grains and through the granular network, the effective thermal conductivity  $\kappa_{\text{eff}}$  is given by

$$\kappa_{\text{eff}}(y) = [x\kappa_g + (1-x)\kappa_v]. \quad (1)$$

Coming back to the Leidenfrost droplet, we assume that if the vapor film thickness (calculated for  $\Delta T$  and in the ideal smooth case) exceeds  $r_{\text{rug}}$ , the vapor flows above the grains without moving them. Indeed, at very high temperatures, it is assumed that the vapor layer is sufficiently thick to flow above the grains and the droplet does not dig, as experimentally observed: The digging speed approaches zero at high temperatures.

Here is the procedure followed. First, we consider the vapor layer thickness  $h_c$  evaluated as if the bulk phase was alone, smooth and at temperature  $\Delta T$ . Then, this thickness is compared to the roughness as defined by the parameter  $r_{\text{rug}}$ . The idea is to recover a classical Leidenfrost droplet at a high temperature, namely, when the film thickness  $h_c$  is larger than the effective roughness  $r_{\text{rug}}$ . However, when  $h_c < r_{\text{rug}}$ , the droplet interacts with the surface layer and the heat is transferred through the granular material located between  $\Sigma_i$  and a parallel plane to  $\Sigma_i$  at a distance  $y = h_c$ . The effective thermal conductivity  $\kappa_{\text{eff}}(y = h_c)$  is then given by the Eq. (1).

In the classical Leidenfrost case, the heat transfer occurs through a vapor film of thickness  $h_c$ , and the vapor production rate is estimated with the following heat equation:

$$Q \sim \frac{\kappa_v}{\mathcal{L}} \frac{S}{h_c} \Delta T, \quad (2)$$

where  $\kappa_v$  is the thermal conductivity of the vapor (0.04 W/m/K),  $\mathcal{L}$  is the latent heat to transform water into vapor and  $S$  is the surface of exchange. Here, half the droplet surface  $S = 2\pi R^2$  is considered. The following equation considers the mass conservation (under the assumption of incompressibility) of the vapor as it flows through a ring of thickness  $h$  around a droplet of radius  $R$ :

$$Q = 2\pi R h_c \rho_v v_v. \quad (3)$$

The vapor speed is governed by the pressure exerted by the weight of the droplet on the bottom half of its surface. The lubrication equation (Navier-Stokes equation neglecting inertia; see Refs. [3,4]) is as follows:

$$\frac{m_d g}{2\pi^2 R^3} \sim \eta_v \frac{v_v}{h_c^2}, \quad (4)$$

where  $m_d$  is the mass of the droplet. Combining the conservation equation Eq. (3) and the lubrication equation Eq. (4), a relation between the superheat and the vapor thickness is obtained, namely,  $h_c \propto \Delta T^{1/4}$ . The hotter the substrate, the thicker the film is. Let us also note that, experimentally, we can evaluate the vapor production regarding the lifetime of the droplet. In the model, the weight of the droplet that is the downward force, is supposed constant. However, two antagonist effects should be considered: On the one hand, the evaporation and, on the other hand, the capture of grains. A fine description is expected. But, regarding the rather linear increase of the depth with time, the constant weight assumption seems to work.

Second, if the thickness  $h_c$  of the vapor film is smaller than the thickness of the surface layer  $r_{\text{rug}}$ , then the droplet directly contacts the granular material. An additional heat flux is transferred directly from the granular material to droplet. Then the vapor production rate is re-evaluated by replacing  $\kappa_v$  with  $\kappa_{\text{eff}}(y = h_c)$  in Eq. (2), and the speed of vapor  $v_v$  is then calculated based on the conservation equation Eq. (3).

Third, since the vapor is generated directly between the grains, we assume that the grains are ejected with a speed equal to the average speed of the vapor in the film of thickness  $h_c$ , namely,  $2v_v/3$  (Poiseuille flow). Moreover, the higher is the droplet (the more  $h_c$  is close to  $r_{\text{rug}}$ ), the more the vapor can escape without entraining grains. To account on this effect, we consider a linear relation  $\Phi = (r_{\text{rug}} - h_c)/r_{\text{rug}}$  that imposes that the grains are not entrained any more when the thickness of the vapor film is larger than the thickness of the surface layer. As a consequence, the speed of the grains  $v_g$  is given by

$$v_g = \frac{2}{3} v_v \Phi. \quad (5)$$

Fourth, the time of escape for the grains is given by  $\pi R/v_g$ . During this time, the droplet penetrates a distance of  $h_c$ . The digging speed is simply given by

$$v_d \sim \frac{h_c}{\pi R} v_g. \quad (6)$$

The above procedure is followed while adjusting the value of  $r_{\text{rug}}$ , such that the grain speed is canceled for a given temperature, which corresponds to  $r_{\text{rug}}=69.5 \pm 0.5$ ,  $71.5 \pm 0.5$ , and  $75 \pm 0.5 \mu\text{m}$  for SiC-I, -II, and -III grains in the Fig. 3(d), respectively. The red, blue and green areas correspond to the calculations for SiC-I, -II, and -III grains, respectively. The value of  $r_{\text{rug}}$  alters the temperature at which the droplet speed is canceled. In other words, above this temperature, the droplet no longer contacts any grains. A rather good agreement is obtained with this simple model. Note that the only fit parameter is  $r_{\text{rug}}$ . This parameter accounts for the grain size, the bigger the grains, the larger  $r_{\text{rug}}$ . Moreover, we can assume that when the packing fraction is large, the speed of digging becomes small. This indicates that the roughness sphere size decreases when the packing fraction increases.

The model also predicts the lifetime as a function of the superheat dividing the droplet mass by the vapor production rate. The lifetime is shown in the inset of Fig. 3(d). The order of magnitude is correctly determined but the predicted lifetime cannot be compared to the penetration duration retrieved from the experiments, as shown in Fig. 3(b). Indeed, the proposed simple model does not consider the time to cross the interface, the trapping process, the influences of both the sapphire window and the back of the Hele-Shaw cell. It is also expected that upward forces are exerted on the droplet due to the flow of grains. The buoyancy force, similar to the fluid hydrostatic force [20], could be considered as well. Finally, since the vapor was produced inside the granular material, we considered that the speed of the grains is given by the speed of the vapor. However, when the temperature is increased, the value of the vapor film thickness increases. The vapor is produced more and more above the grains located at the surface of the granular material. A more sophisticated model should be considered by implementing a coupling between the vapor and the grain such as found in the review by Dey *et al.* [21].

## V. CONCLUSION

We report the behavior of liquid droplets released onto a deep granular bed when the temperature is far above the boiling temperature of the liquid. We find that the droplet digs in the granular bed at a constant speed, which depends nonlinearly on the temperature. Visualization with a Hele-Shaw cell facilitated the monitoring of the precise trajectory of the droplet and determination of the penetration mechanism. At temperatures just above the boiling temperature, the droplet contacts the grains, thereby producing a large amount of vapor that locally fluidises the granular bed just below the droplet. At higher temperatures, the vapor layer expands as more gas is produced. As a consequence, less and less grains are touched by the droplet. The resultant heat transfer is therefore also reduced. Eventually, when the temperature is high enough, the classical Leidenfrost state is nearly reached, namely, the droplet levitates above the granular bed.

The cooling process of the grain assembly by a liquid exhibits different dynamics according to the temperature difference between the cooling liquid and grains. We revealed that a temperature range above the boiling temperature of the liquid is particularly favorable for efficient cooling of the grains because the droplets deeply penetrate into the granular material, thereby cooling the interior of the material.

---

[1] J. Leidenfrost, *De Aquae Communis Nonnullis Qualitatibus Tractatus* (Ovenius, Duisburg, 1756).

[2] P. Boutigny, *Dictionnaire des arts et manufactures: Description des procédés de l'industrie française et étrangère* (Librairie Scientifique et Industrielle de L. Mathias, Paris, 1847).

[3] A. L. Bianco, C. Clanet, and D. Quéré, Leidenfrost dynamics, *Phys. Fluids* **15**, 1632 (2003).

- [4] D. Quéré, Leidenfrost dynamics, *Annu. Rev. Fluid Mech.* **45**, 195 (2013).
- [5] H.-m. Kwon, J. Bird, and K. K. Varanasi, Increasing Leidenfrost point using micro-nano hierarchical surface structures, *Appl. Phys. Lett.* **103**, 201601 (2013).
- [6] H. Kim, B. Truong, J. Buongiorno, and L. Hu, On the effect of surface roughness height, wettability, and nanoporosity on Leidenfrost phenomena, *Appl. Phys. Lett.* **98**, 083121 (2011).
- [7] L. Maquet, B. Sobac, B. Darbois-Textier, A. Duchesne, M. Brandenbourger, A. Rednikov, P. Colinet, and S. Dorbolo, Leidenfrost drops on a heated liquid pool, *Phys. Rev. Fluids* **1**, 053902 (2016).
- [8] B. Sobac, L. Maquet, A. Duchesne, H. Machrafi, A. Rednikov, P. Dauby, P. Colinet, and S. Dorbolo, Self-induced flows enhance the levitation of Leidenfrost drops on liquid baths, *Phys. Rev. Fluids* **5**, 062701(R) (2020).
- [9] E. Guyon, J.-Y. Delenne, and F. Radjai, *Built on Sand The Science of Granular Materials* (MIT Press, 2020).
- [10] D. Liu, T.-B. Nguyen, N.-V. Nguyen, and T. Tran, Sailing Droplets in Superheated Granular Layer, *Phys. Rev. Lett.* **125**, 168002 (2020).
- [11] G. McHale, M. Newton, and N. Shirtcliffe, Water-repellent soil and its relationship to granularity, surface roughness and hydrophobicity: A materials science view, *Eur. J. Soil Sci.* **56**, 445 (2005).
- [12] D. Polamuri and S. Thamida, Experimental determination of effective thermal conductivity of granular material by using a cylindrical heat exchanger, *Int. J. Heat Mass Transf.* **81**, 767 (2015).
- [13] E. Huetter, N. Koemle, G. Kargl, and E. Kaufmann, Determination of the effective thermal conductivity of granular materials under varying pressure conditions, *J. Geophys. Res.* **113**, E12004 (2008).
- [14] G. Delon, D. Terwagne, S. Dorbolo, N. Vandewalle, and H. Caps, Impact of liquid droplets on granular media, *Phys. Rev. E* **84**, 046320 (2011).
- [15] S. Zhao, R. de Jong, and D. van der Meer, Raindrop impact on sand: A dynamic explanation of crater morphologies, *Soft Matter* **11**, 6562 (2015).
- [16] S.-C. Zhao, R. de Jong, and D. van der Meer, Liquid-Grain Mixing Suppresses Droplet Spreading and Splashing During Impact, *Phys. Rev. Lett.* **118**, 054502 (2017).
- [17] L. Maquet, P. Colinet, and S. Dorbolo, Organization of microbeads in Leidenfrost drops, *Soft Matter* **10**, 4061 (2014).
- [18] See Supplemental Material at <http://link.aps.org/supplemental/10.1103/PhysRevFluids.7.034301> for additional descriptions of the properties of the grains, the thermal analysis, and further analysis of the digging speed and the vapor production.
- [19] Y.-W. Kim, K.-Y. Lim, and W.-S. Seo, Microstructure and thermal conductivity of silicon carbide with yttria and scandia, *J. Am. Ceram. Soc.* **97**, 923 (2013).
- [20] D. A. Huerta, V. Sosa, M. C. Vargas, and J. C. Ruiz-Suárez, Archimedes' principle in fluidized granular systems, *Phys. Rev. E* **72**, 031307 (2005).
- [21] S. Dey and S. Zeeshan Ali, Advances in modeling of bed particle entrainment sheared by turbulent flow, *Phys. Fluids* **30**, 061301 (2018).